Journal of Applied Physics

RESEARCH ARTICLE | JULY 08 2024

Influence of local structures on amorphous alumina exhibiting resistance random-access memory function

Masato Kubota ; Seiichi Kato

J. Appl. Phys. 136, 025102 (2024)
https://doi.org/10.1063/5.0208486

AIP Publishing

Journal of Applied Physics ARTICLE pubs.aip.org/aip/jap

Influence of local structures on amorphous alumina exhibiting resistance random-access memory function

Cite as: J. Appl. Phys. **136**, 025102 (2024); doi: 10.1063/5.0208486
Submitted: 27 March 2024 · Accepted: 11 June 2024 ·
Published Online: 8 July 2024

Masato Kubota[1,a)] and Seiichi Kato[2]

AFFILIATIONS

[1]Japan Atomic Energy Agency (JAEA), 2-4 Shirakata Tokai-mura, Naka-gun, Ibaraki 319-1195, Japan
[2]International Center for Materials Nanoarchitectonics (MANA), National Institute for Materials Science (NIMS), 1-1 Namiki, Tsukuba, Ibaraki 305-0044, Japan

[a)]**Author to whom correspondence should be addressed:** kubota.masato@jaea.go.jp

ABSTRACT

Amorphous alumina resistance random-access memory is a promising candidate as a next-generation nonvolatile memory. It is intriguing that the nonvolatile memory function emerges in only amorphous samples, unlike crystalline samples. We studied local structures of amorphous alumina samples and Al_2O_3 polycrystalline using atomic pair distribution function measurements. We derived the Al–Al, O–O, and Al–O atomic distances for each sample. By comparing them, we revealed that the subtle difference in the local structure significantly influences the performance of a nonvolatile memory function.

I. INTRODUCTION

According to the evolution of a modern information intensive society, the mass consumption of electric power is a pressing issue.[1–3] One effective way to resolve this problem is to prevalently use a next-generation high-performance nonvolatile memory system. Resistance random-access memory (ReRAM) with resistance switching operated by voltage is a promising candidate for the next-generation nonvolatile memory. In the recent development of the ReRAM, many transition metal-based ReRAM materials, such as NiO and Ta_2O_5, are intensively investigated.[4–9] However, there are several conclusively disadvantageous matters for the performance of the nonvolatile memory. For instance, a large leakage current is a weak point in NiO, whereas a chemical reaction is accompanied by minor reactions that generate by-products in Ta_2O_5. Deteriorating factors, such as by-products and/or an oxygen ion movement in a chemical reaction, reduce the endurance of the transition metal-based ReRAM device. Furthermore, an additional forming process is indispensable to generate a preliminary conducting path, which is disadvantageous for the mass production of memory devices.

We study amorphous alumina-based ReRAM (AlO-ReRAM) without transition metals, which cause the deterioration of the nonvolatile memory function. We accomplished the top-class functionality with high speed (5 ns) and low power consumption (28 μA).[10] In addition, many advantageous features exist, such as a large On/Off resistance ratio ($\sim 10^{-9}$),[11] no requirement of an additional forming process, and the exclusion of rare and noxious elements for developing the AlO-ReRAM in the near future.[12]

We propose the oxygen vacancy model for the electrical property in the AlO-ReRAM.[10,12] In this model, it is expected that the charge/discharge (On/Off) switching of the nonvolatile memory results from the changes of electron cloud overlap/isolation between oxygen vacancy clusters, where a conducting path can be formed. Consequently, injecting external electrons around an oxygen vacancy form the energy subband in a metallic state, whereas extracting electrons diminish the subband in an insulating state. This model has several fingerprints for verification. We detected a change in the electronic structure between high and low resistance states and demonstrated that AlO-ReRAM shows no chemical reaction or by-products in the x-ray absorption spectra.[12] A subpeak for the charging of electrons into oxygen vacancies was

observed between the valence and conduction bands. It is also recognized that the energy potential for the electron around the oxygen vacancy is stable, revealed by the first-principles calculation.[13]

We clarified that only amorphous alumina shows a nonvolatile memory function, unlike polycrystalline alumina.[10,11] The first-principles calculation exhibits that the energy level of the subband (midgap) changes depending on the electronic states in amorphous alumina, whereas the energy level in polycrystalline alumina is robust.[13] The calculation also shows that the change in the electronic states is accompanied by subtle structural relaxation due to the change in the local structure in amorphous alumina. Based on these theoretical suggestions, we expect that the local structure in the Off state essentially affects the presence or absence of the nonvolatile memory function and the superiority or inferiority of the function.

Considering these things, to experimentally reveal the relationship between the local structure in the Off state and the feature of the nonvolatile memory function, we perform atomic pair distribution function (PDF) measurements on two types of amorphous samples with good/less switching performance of the nonvolatile memory function. For comparison, PDF measurement is also performed for Al_2O_3 polycrystalline, which exhibits no effect of nonvolatile memory.

II. EXPERIMENT

Two amorphous alumina samples were prepared using anodic oxidation. Alumina material (4N) was oxidized in 0.3 M oxalic acid at 40 V (sample A), and 0.3 M phosphoric acid at 130 V (sample B), in the same sample preparation noted in Ref. 14. In current–voltage measurements, sample A with a thickness of approximately 5 μm shows switching performance of nonvolatile memory by applying an electric voltage of 60 V, whereas sample B exhibits no performance, even by applying up to 70 V. We separated anodized alumina from a raw aluminum material using the voltage reversal technique. The only anodized alumina is grinded into powder for the PDF measurements. The Al_2O_3 polycrystalline powder (4 N) is also measured as a reference sample.

The high energy x-ray PDF measurements were performed on the amorphous samples and the polycrystalline at the BL04B2 beamline at the SPring-8 synchrotron radiation facility.[15,16] The incident x-ray energy was 61.36 keV with the energy resolution $\Delta E/E$ of approximately 5×10^{-3}. We meticulously addressed to reduce truncation effects and related errors by the measurements with the low statistical noise and the extended Q-range, as noted in Ref. 17 Notably, the dedicated diffractometer of BL04B2 yields high-quality data through step-scan measurements, where the background noise is extremely small. The measuring time is so long that the magnitude of the statistical noise is less than 0.2% of that of the signal for the total structure factor in the whole Q-range. In addition, it is generally recognized that the scan Q-range up to 28 Å^{-1} (Q_{max}) in this study is wide enough to analyze the accurate PDF data.

The diffractometer features three Ge detectors (GL-0515R, Cambella, USA) accompanied with an automated liquid nitrogen filling system and four CdTe detectors (X-123CdTe, Amptek, USA).[15] The supersensitivity of a Ge detector is advantageous for the measurements in the high-diffraction-angle region, because the diffraction intensity is weak in the high-diffraction-angle region due to the decay of Q-dependent atomic form factors. Conversely, the smallness of a CdTe detector is advantageous for covering a low-diffraction-angle region in a limited space. Additionally, the semiconductor detectors provide high energy resolution to discriminate the fluorescence from the sample and the signal of the higher harmonic reflection of the monochromator crystal, which are essential for obtaining accurate PDF data. Furthermore, the limited flight path with a double-slit system is employed for minimizing the background scattering from the experimental surroundings. Consequently, our observed data are sufficiently reliable for the analyses.

The samples were transferred into quartz capillaries, with the diameter of 2 mm. The sample changer combined with a fully automated alignment system is utilized to exchange the quartz capillaries containing the samples, which causes no difference of each sample position for an x-ray beam without experimental ambiguity. We used the reliable software package of "BL04B2anaGUI" for PDF data extraction, which is widely utilized by many researchers at beamline BL04B2 in SPring-8.[16,18–21] The raw data were corrected for polarization, absorption, and background, and the contribution of Compton scattering was subtracted.

III. RESULTS AND DISCUSSION

Figure 1(a) compares the x-ray total structure factors of $S(Q)_A$ for sample A and $S(Q)_B$ for sample B. The profiles in the amorphous samples are broad and weak. As similar features in $S(Q)_A$ and $S(Q)_B$, two local maxima appear around $Q = 2.2$ Å^{-1} and 2.9 Å^{-1} (first and second peaks). The center positions of the profiles for sample A around $Q \sim 4.4$ Å^{-1} (third peak) and ~ 7.6 Å^{-1} (fourth peak) are located lower than those for sample B (dashed arrows), respectively, whereas the center position of the profile around $Q \sim 11.2$ Å^{-1} (fifth peak) for sample A is similar to that for sample B. For sample B, a shoulder in the profile can be observed around $Q = 6.7$ Å^{-1}. Figure 1(b) shows the total structure factor $S(Q)_{Al_2O_3}$ for Al_2O_3 polycrystalline, where sharp and strong profiles corresponding to Bragg reflections are observed in contrast with $S(Q)_A$ and $S(Q)_B$.

It is well-known that the first sharp diffraction peak (FSDP) is observed in a total structure factor of typical glass-forming materials, such as SiO_2, originating from successive small structural cages reproduced by voids.[22–24] However, the profiles around $Q = 2.2$ Å^{-1} in $S(Q)_A$ and $S(Q)_B$ are extremely broad, meaning that FSDPs are absent in both amorphous alumina samples. This result reflects that the cages of oxide polyhedra reproduced by oxygen void and surrounding Al and O atoms (oxygen vacancy cluster) are significantly disordered, and the correlation of the oxygen vacancy clusters remains short-ranged in both samples.

We obtain corresponding real space information, such as atomic distances, using the reduced PDF $G(r)$, which is defined as

$$G(r) = \frac{2}{\pi}\int_{Q_{min}}^{Q_{max}} Q[S(Q) - 1]\sin(Qr)dQ,$$

where r is the distance in real space. Q_{min} and Q_{max} in this study

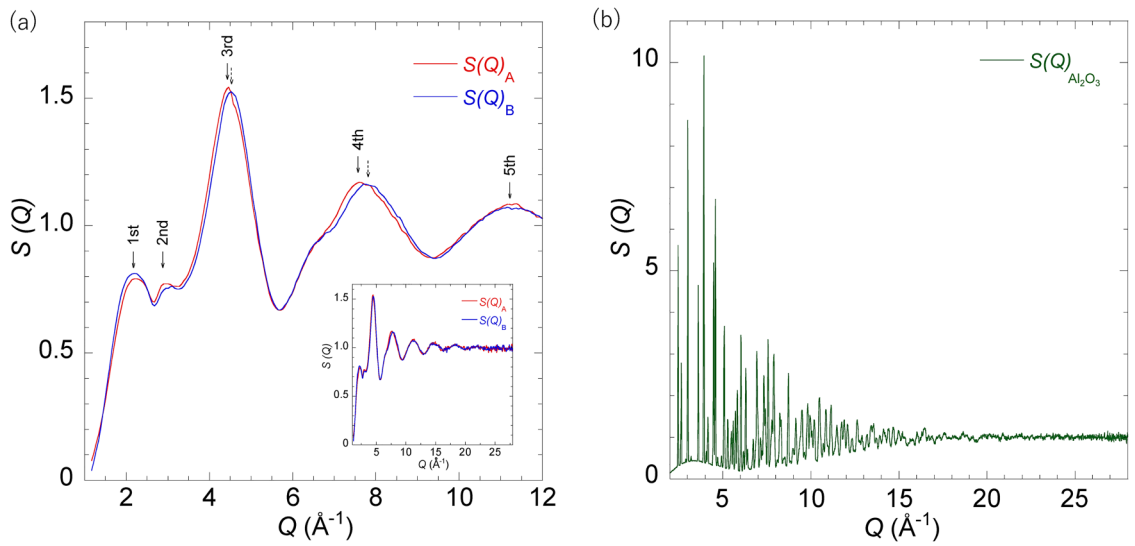

FIG. 1. (a) Comparison of the x-ray total structure factor $S(Q)$ for samples A [$S(Q)_A$] and B [$S(Q)_B$]. The solid (dashed) arrows show the center positions of the profiles for sample A (sample B). The inset shows $S(Q)_A$ and $S(Q)_B$ in a whole Q range. (b) Total structure factor $S(Q)_{Al_2O_3}$ for Al_2O_3 polycrystalline.

are 0.2 and 28, respectively. In the calculation of $G(r)$, the Lorch window function is used.[16,25]

Figure 2 shows the reduced PDFs $G(r)$ for sample A, sample B, and Al_2O_3 polycrystalline. For the polycrystalline, clear profiles

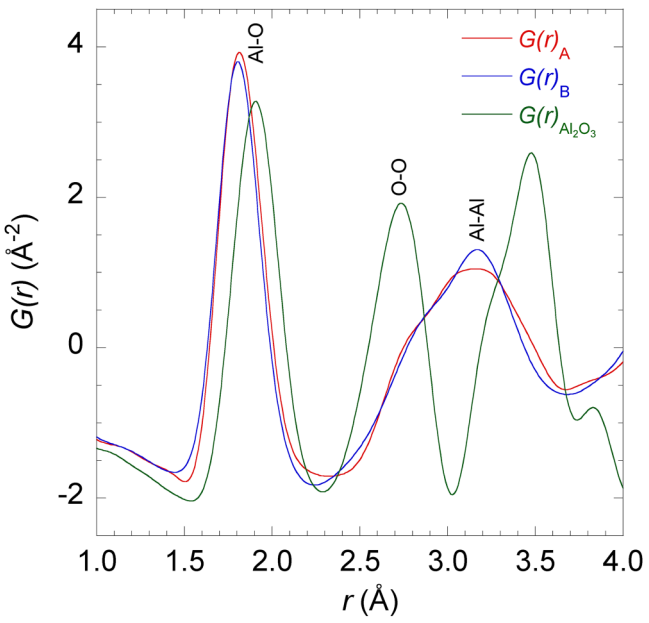

FIG. 2. Comparison of reduced PDFs $G(r)$ for samples A [$G(r)_A$], B [$G(r)_B$], and Al_2O_3 polycrystalline [$G(r)_{Al_2O_3}$].

are observed at 1.91(1) and 2.73(2) Å. These center positions of the profiles correspond to the Al–O and O–O atomic distances, respectively, whereas the shoulder around 3.23(3) Å corresponds to the Al–Al atomic distance, based on the assigned profiles as referenced in Refs. 19 and 26 In a similar way, for sample A, the center position of the profile at 1.81(1) Å is assigned to the Al–O atomic distance. From the local maximum and the center position of the profile, it is revealed that the O–O atomic distance is around 2.73 (4), and the Al–Al atomic distance is approximately 3.15(4) Å. For sample B, the Al–O, O–O, and Al–Al atomic distances are 1.81(1), 2.83(4), and 3.18(2) Å, respectively.

In Al_2O_3 polycrystalline, the coordination number of oxygen around aluminum is six. However, aluminum with the coordination number of four and five also exist within the amorphous samples, including six, by NMR measurements.[14] We evaluated the Al–O coordination number through the observed data for the amorphous samples. The evaluated Al–O coordination number is 5.0(2). This value is consistent with the coordination number of approximately 4.9 revealed by NMR in the amorphous samples,[14] which were prepared in the same way as this study.

A typical glass-forming material, SiO_2, forms successive small cages with the network of regular SiO_4 tetrahedra with shared oxygen atoms at the corners, where the periodicity of the boundaries of the cages is clear. The coordination number of SiO_2 polyhedra is four.[20] However, it is well-known that the periodicity of the boundaries in the liquid-Al_2O_3 cluster is unclear due to the large contribution of AlO_5 polyhedra.[20] Considering these things, it can be safely said that the boundary of the oxygen vacancy clusters is disturbed in the amorphous sample because the Al′O coordination number is approximately five, as mentioned above. This result is consistent with the suppression of the FSDP in the amorphous samples [Fig. 1(a)].

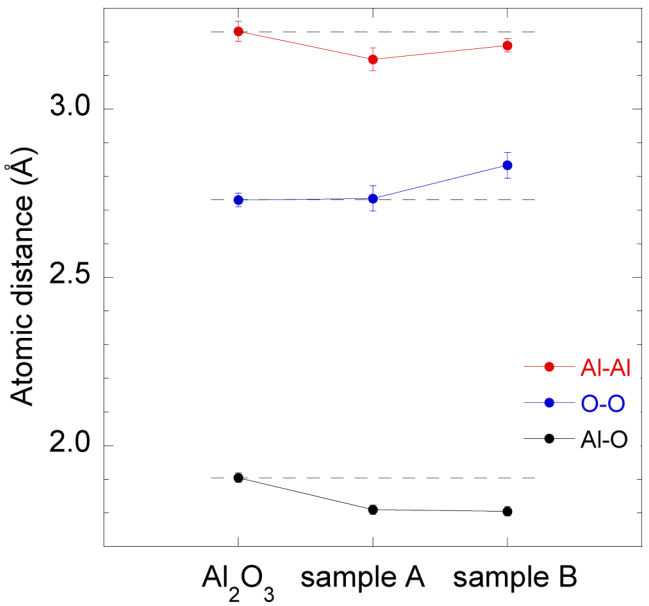

FIG. 3. Comparison of the atomic distances of Al–Al, O–O, and Al–O for samples A, B, and Al_2O_3 polycrystalline. The horizontal broken line is a guide to the eyes for the comparison.

Figure 3 compares the atomic distances for Al–Al, O–O, and Al–O in the three samples. First, we compare the features of the atomic distances between the polycrystalline and sample A. The Al–Al atomic distance in sample A is 2.5% shorter than that in the polycrystalline, and the Al–O atomic distance in the former is 5.2% shorter than that in the latter. The O–O atomic distance of sample A is similar to that of the polycrystalline. Oxygen is deficient in the amorphous samples, unlike the polycrystalline sample. In a simple viewpoint, the oxygen deficiency elongates the O–O atomic distance. Since the oxygen in sample A is deficient, it is expected that the O–O atomic distance in sample A is longer than that in the polycrystalline. However, the O–O atomic distances for both samples are surprisingly similar in Fig. 3. This result effectively means that the distance of the O–O atomic distance within an oxygen vacancy cluster in sample A further shortens, compared with that in the polycrystalline.

Successively, to reveal the role of the atomic distances in amorphous alumina accompanied with the nonvolatile memory function, we compare the features of the atomic distances between samples A and B. Oxygen vacancies exist in the amorphous samples. The amount of oxygen vacancies in sample B is larger than that in sample A, as noted in Ref. 14. The most noticeable point is that the O–O atomic distance in sample B is approximately 3.7% elongated against the polycrystalline, in contrast with that in sample A. The Al–Al and Al–O atomic distance in sample B are shortened against the polycrystalline. In more detail, the Al–Al atomic distance in sample B is approximately 1% longer than that in sample A. The Al–O atomic distance in sample B is similar to that in sample A, indicating that the different amorphization has little influence on the Al–O atomic distance.

The relationship between the nonvolatile memory function and the local structure is theoretically examined by focusing on the change in the size of the oxygen vacancy cluster, which necessarily causes the change in the atomic distances.[13] Considering that a nonvolatile memory function never emerges in a polycrystalline sample, appropriate requirements for the atomic distances in the Off state below a specific value are likely to produce the switching performance in an amorphous sample. An amorphous alumina sample is more suitable for a ReRAM material than a polycrystalline sample because the energy levels and local structures in the former sample are more sensitive to the change in the electronic state than those in the latter sample.[13]

By comparison, the Al–Al atomic distance in sample A is 0.03 Å shorter than that in sample B, whereas the O–O atomic distance in sample A is 0.1 Å shorter than that in sample B (Fig. 3). Sample A shows better switching performance of nonvolatile memory than sample B. Therefore, it is likely that short Al–Al and O–O atomic distances are advantageous for the emergence of the switching performance. It could be that the good switching performance of the nonvolatile memory function occurs in sample A since the short atomic distances can easily cause electron clouds to be overlapped between oxygen vacancy clusters. This is consistent with the theoretical suggestion of the local structure.[13]

It is experimentally revealed that even the subtle difference in the local structure in the Off state is crucial for the nonvolatile memory function of amorphous alumina, mentioned above. Combined with the first-principles calculation,[13] it is suggestive that AlO-ReRAM works based on the oxygen vacancy model, which shows possible high endurance. This suggestion is in contrast with the fact that chemical reactions accompanied with by-products and/or an oxygen ion movement deteriorate transition metal-based ReRAM. In addition, high speed and low power consumption are realized, and no by-product exists in AlO-ReRAM.[10–12] We believe that the knowledge obtained in this study is vital for the development of high-performance AlO-ReRAM.

IV. CONCLUSIONS

In conclusion, we performed PDF measurements on amorphous alumina samples and Al_2O_3 polycrystalline to reveal their local structures. We obtained the Al–Al, O–O, and Al–O atomic distances for each sample. By comparing these atomic distances, we revealed their conditions in the Off state for showing the nonvolatile memory function. We clarified that even the subtle difference in the local structure in the Off state influences the performance of the nonvolatile memory function in amorphous alumina.

ACKNOWLEDGMENTS

We gratefully thank Dr. H. Yamada, Dr. J. Tseng, Dr. S. Nigo, and Dr. K. Kodama for their technical support and fruitful discussions. The x-ray experiment was performed under approval of the SPring-8 Proposal Review Committee (Proposal Nos. 2023A1275 and 2024A1413).

AUTHOR DECLARATIONS

Conflict of Interest

The authors have no conflicts to disclose.

Author Contributions

Masato Kubota: Conceptualization (lead); Data curation (lead); Formal analysis (lead); Investigation (equal); Methodology (lead); Supervision (equal); Writing – original draft (lead); Writing – review & editing (equal). **Seiichi Kato:** Investigation (equal); Supervision (equal); Writing – original draft (supporting); Writing – review & editing (equal).

DATA AVAILABILITY

The data that support the findings of this study are available from the corresponding author upon reasonable request.

REFERENCES

[1]L. Belkhir and A. Elmeligi, J. Clean. Prod. **177**, 448 (2018).
[2]A. S. G. Andrae and T. Edler, Challenges **6**, 117 (2015).
[3]T. Bawdy, "Global warming: Data centres to consume three times as much energy in next decade, experts warn," *The Independent*, 23 January 2016.
[4]J. F. Gibbons and W. E. Beadle, Solid-State Electron. **7**, 785 (1964).
[5]I. G. Baek, M. S. Lee, S. Seo, M. J. Lee, D. H. Seo, D.-S. Suh, J. C. Park, S. O. Park, H. S. Kim, I. K. Yoo, U.-I. Chung, and J. T. Moon, in *International Electron Devices Meeting. IEDM Technical Digest* (IEEE, 2004), p. 587.
[6]C. Yoshida, K. Kinoshita, T. Yamasaki, and Y. Sugiyama, Appl. Phys. Lett. **93**, 042106 (2008).
[7]Z. Wei, Y. Kanzawa, K. Arita, Y. Katoh, K. Kawai, S. Muraoka, S. Mitani, S. Fujii, K. Katayama, M. Iijima, T. Mikawa, T. Ninomiya, R. Miyanaga, Y. Kawashima, K. Tsuji, A. Himeno, T. Okada, R. Azuma, K. Shimakawa, H. Sugaya, T. Takagi, R. Yasuhara, K. Horiba, H. Kumigashira, and M. Oshima, in *International Electron Devices Meeting. IEDM Technical Digest* (IEEE, 2008), p. 293.
[8]Y. Sakotsubo, M. Terai, S. Kotsuji, T. Sakamoto, and M. Hada, Jpn. J. Appl. Phys. **49**, 04DD19 (2010).
[9]B. Y. Kim, W. G. Kim, H. J. Kim, K. H. Jung, W. Y. Park, B. M. Seo, M. S. Joo, K. J. Lee, K. Hong, and S. K. Park, Jpn. J. Appl. Phys. **52**, 04CD05 (2013).
[10]S. Nigo, M. Kubota, Y. Harada, T. Hirayama, S. Kato, H. Kitazawa, and G. Kido, J. Appl. Phys. **112**, 033711 (2012).
[11]S. Kato, S. Nigo, Y. Uno, T. Onisi, and G. Kido, J. Phys. Conf. Ser. **38**, 148 (2006).
[12]M. Kubota, S. Nigo, S. Kato, and K. Amemiya, AIP Adv. **9**, 095050 (2019).
[13]H. Momida, S. Nigo, G. Kido, and T. Ohno, Appl. Phys. Lett. **98**, 042102 (2011).
[14]T. Iijima, S. Kato, R. Ikeda, S. Ohki, and G. Kido, Chem. Lett. **34**, 1286 (2005).
[15]H. Yamada, K. Nakada, M. Takemoto, and K. Ohara, J. Synchrotron Radiat. **29**, 549 (2022).
[16]K. Ohara, S. Tominaka, H. Yamada, M. Takahashi, H. Yamaguchi, F. Utsuno, T. Umeki, A. Yao, K. Nakada, M. Takemoto, S. Hiroi, N. Tsuji, and T. Wakihara, J. Synchrotron Radiat. **25**, 1627 (2018).
[17]L. B. Skinner, S. C. Huang, D. Schlesinger, L. G. M. Pettersson, A. Nilsson, and C. J. Benmore, J. Chem. Phys. **138**, 074506 (2013).
[18]L. C. Gallington, S. K. Wilke, S. Kohara, and C. J. Benmore, Quantum Beam Sci. **7**, 20 (2023).
[19]K. Ohara, Y. Onodera, M. Murakami, and S. Kohara, J. Phys.: Condens. Matter **33**, 383001 (2021).
[20]S. Kohara, J. Akola, L. Patrikeev, M. Ropo, K. Ohara, M. Itou, A. Fujiwara, J. Yahiro, J. T. Okada, T. Ishikawa, A. Mizuno, A. Masuno, Y. Watanabe, and T. Usuki, Nat. Commun. **5**, 5892 (2014).
[21]K. Kojima, N. Katayama, Y. Matsuda, M. Shiomi, R. Ishii, and H. Sawa, Phys. Rev. B **107**, L020101 (2023).
[22]D. L. Price, S. C. Moss, R. Reijers, M. L. Saboungi, and S. Susman, J. Phys. C: Solid State Phys. **21**, L1069 (1988).
[23]T. Uchino, J. D. Harrop, S. N. Taraskin, and S. R. Elliott, Phys. Rev. B **71**, 014202 (2005).
[24]P. H. Gaskell and D. J. Wallis, Phys. Rev. Lett. **76**, 66 (1996).
[25]E. Lorch, J. Phys. C: Solid State Phys. **2**, 229 (1969).
[26]L. B. Skinner, A. C. Barnes, P. S. Salmon, L. Hennet, H. E. Fischer, C. J. Benmore, S. Kohara, J. K. R. Weber, A. Bytchkov, M. C. Wilding, J. B. Parise, T. O. Farmer, I. Pozdnyakova, S. K. Tumber, and K. Ohara, Phys. Rev. B **87**, 024201 (2013).